AIAA 98–2220

Numerically Nonreflecting Boundary Conditions for Multidimensional Aeroacoustic Computations

Clarence W. Rowley and Tim Colonius
Division of Engineering and Applied Science
California Institute of Technology
Pasadena, CA 91125

4th AIAA/CEAS Aeroacoustics Conference
June 2-4, 1998 / Toulouse, France

NUMERICALLY NONREFLECTING BOUNDARY CONDITIONS FOR MULTIDIMENSIONAL AEROACOUSTIC COMPUTATIONS

Clarence W. Rowley and Tim Colonius
Division of Engineering and Applied Science
California Institute of Technology
Pasadena, CA 91125

Abstract

Many compressible flow and aeroacoustic computations rely on accurate nonreflecting or radiation boundary conditions. When the equations and boundary conditions are discretized using a finite-difference scheme, the dispersive nature of the discretized equations can lead to spurious numerical reflections not seen in the continuous boundary value problem. These reflections can lead to poor convergence to a stationary state, and can lead to self-forcing of flows. We have constructed numerically nonreflecting boundary conditions which account for the particular finite-difference scheme used, and are designed to minimize these spurious numerical reflections. These extend our earlier work on one-dimensional boundary conditions to the multidimensional case. Stable boundary conditions which are nonreflecting to arbitrarily high-order-of-accuracy are obtained. Various test cases are presented which show excellent results.

1 Introduction

The development of accurate and robust nonreflecting boundary conditions has been one of the principle difficulties in the development of computational aeroacoustic codes [1, 2, 3]. The basic goal of such boundary conditions is to truncate computational domains for problems which are defined on a infinite or semi-infinite space. Ideally, the computational domain would need only include regions of the flow where significant production of acoustic waves occurs, or where the acoustic field is scattered or refracted by nonuniform flow conditions or solid bodies. Outside such a region, the acoustic waves are (in many cases) governed by linear equations whose solution can be written in terms of integrals.

Boundary conditions have typically been developed by first constructing the boundary conditions for the continuous equations, and then discretizing them in an ad hoc way, for example by using one-sided differences for derivatives near the boundary. This approach can lead to serious inaccuracy and/or instability because it does not recognize that discretizations of hyperbolic equations are usually dispersive, and waves which are resolved with varying numbers of grid points propagate at different speeds, e.g. [4, 5]. While boundary conditions which account for this dispersive nature have been developed in some special cases [6, 7], there is no general formulation for the linearized Euler equations (LEE).

The goal of this paper is to present a generalized framework which we have developed for constructing numerically (discretely) nonreflecting boundary conditions for LEE. We have derived stable boundary conditions which can be extended to arbitrarily high order-of-accuracy. Both physical reflections (due to local approximations in the modified dispersion relations) and spurious numerical reflections (due to dispersive effects at finite resolutions) may be minimized in this approach. There are some tradeoffs (numerical nonreflectivity vs. physical nonreflectivity) which depend on the specific problem under consideration, but in general we show that the performance of the boundary conditions is excellent. Many of the details of the analysis are algebraically complicated, and are beyond the scope of this paper. Here we will simply outline the steps necessary to derive the conditions and present the results of various tests of their accuracy. The reader is referred to our manuscript [8] (which may be obtained at http://green.caltech.edu/tc.html) for the details.

This paper is organized as follows. In section 2 we describe the approximations we use to construct local continuous boundary conditions for the LEE. These schemes, by themselves, give very accurate results when discretized in a typical ad hoc way. By this we mean that the boundary conditions and interior points are discretized using biased or one-sided finite-difference (FD) approximations near the boundary when derivatives normal to the boundary are needed. However, more robust and accurate discrete boundary conditions are derived in section 3, by explicitly considering the dispersive nature of the FD discretization at the outset. Thus we construct numerically nonreflecting conditions. These latter schemes are, of necessity, restricted to particular FD schemes, and we choose the standard three point central FD (both explicit and Padé) to illustrate the

analysis. The results of various test cases are presented in section 4. A brief summary of the results and directions for future work are given in section 5.

2 Continuous Boundary Conditions

2.1 Background

Two distinct approaches have been used in deriving boundary conditions for the continuous LEE. We briefly review the basic ideas — recent reviews [9, 10, 1] give further references to the relevant literature [9].

The first method involves so-called radiation boundary conditions, which are based on asymptotic expansions of the solution produced by a finite source region. Very accurate local and nonlocal boundary conditions based on this expansion have been developed for the wave equation (e.g. [11]), but radiation techniques for the linearized Euler equations [12, 10] are more limited. In a comparison [13] of many different boundary conditions, the accuracy of these conditions were found to be roughly comparable to Giles boundary conditions, discussed below.

The second technique goes back to the early work on Enquist and Majda [14, 15] and involves the decomposition of the solution in a linear region into Fourier/Laplace modes. Exact boundary conditions are then constructed by eliminating those modes which have a group velocity which is directed into the computational domain. The exact conditions are nonlocal in space and time, but local approximations to these can be constructed. These involve rational function approximations to $\sqrt{1-z^2}$, where z is the wavenumber in the direction tangent to the boundary divided by the frequency of the wave. Note that multiplication of a variable by $\sqrt{1-z^2}$ in Fourier Space corresponds to a nonlocal operation in real space. The function $\sqrt{1-z^2}$ arises when the dispersion relation for acoustic waves is split into incoming and outgoing modes at a boundary. For the simple wave equation, Trefethen and Halpern [16] have developed a theory which shows that certain rational function approximations lead to stable boundary conditions. These *do not* include Taylor series expansions (TSE) about $z = 0$ higher than second-order. However stable Padé approximations can be constructed which *reproduce* the TSE to arbitrarily high order. The Padé approximations are exact for normal waves, and give the highest error for waves whose group velocity is tangent to the boundary.

Unfortunately, the extension of the results for the simple wave equation to the LEE has not been straightforward. Giles [17] found that the second-order TSE of the modified dispersion relation led to ill-posed boundary conditions. By an ad hoc procedure, he modified these conditions to obtain boundary conditions which are stable, but have limited accuracy.

More recently, Goodrich and Hagstrom [18] described inflow and outflow boundary conditions for the LEE which are well-posed for arbitrarily high accuracy. Hagstrom [19] has also developed a series of nonlocal boundary conditions, and a local approximation which is equivalent to the Padé approximation to $\sqrt{1-z^2}$. Using a somewhat different approach, described in more detail in section 2.2, we have derived a similar hierarchy. Interestingly, the proof of well-posedness for our boundary conditions leads to conditions on rational function approximations to the square root which are identical to those derived for the simple wave equation by Trefethen and Halpern [16]. This opens the possibility of a wide variety of boundary conditions which may be specifically tailored to the problem at hand. We give an example of such a scheme in section 4.

2.2 Analysis

The starting point for the analysis is the isentropic linearized Euler equations. We write them in a matrix form, using the *one-dimensional characteristic variables*, $q = (v, u+p, u-p)$, where u and v are the velocities in the x and y directions, respectively, which have been normalized with respect to the constant sound speed of the base flow. The pressure p is normalized by the ambient density times the sound speed squared. For simplicity we consider the two-dimensional case: the extension to three spatial dimensions is straightforward. The equations are:

$$q_t + Aq_x + Bq_y = 0 \tag{1}$$

where

$$A = \begin{pmatrix} U & 0 & 0 \\ 0 & U+1 & 0 \\ 0 & 0 & U-1 \end{pmatrix}, \qquad B = \begin{pmatrix} V & 1/2 & -1/2 \\ 1 & V & 0 \\ -1 & 0 & V \end{pmatrix}$$

where U and V are the Mach numbers of the uniform base flow in the x and y directions. Lengths are made dimensionless with an (as yet unspecified) length L, and time is made dimensionless with L and the sound speed. Note that we may transform to a new set of independent variables in which the uniform velocity in the normal direction is zero. That is, we take $t' = t + y/V$.

Assuming $0 < U < 1$ (subsonic flow), the matrix A is invertible:

$$q_x = -A^{-1}(q_{t'} + Bq_y)$$

We take a Fourier transform in y and a Laplace transform in time, with (ik, s) the dual variables of (y, t'), gives

$$\hat{q}_x = -sM(z)\hat{q} \tag{2}$$

where $z = ik/s$, $\hat{q}$ is the transform of q, and

$$M(z) = \begin{pmatrix} \frac{1}{U} & \frac{z}{2U} & \frac{-z}{2U} \\ \frac{z}{U+1} & \frac{1}{U+1} & 0 \\ \frac{-z}{U-1} & 0 & \frac{1}{U-1} \end{pmatrix}. \tag{3}$$

The eigenvalues of $M(z)$ are

$$\lambda_1 = 1/U$$
$$\lambda_{2,3} = (U \mp \gamma)/(U^2 - 1)$$

where $\gamma(z) = \sqrt{1 - z^2(1 - U^2)}$, and where the standard branch of the square root is used. The x-components of the group velocities of these modes are found:

$$c_{g_1} = U$$
$$c_{g_{2,3}} = (U^2 - 1)/(U \mp 1/\gamma)$$

Note that solutions are waves when $z, \gamma \in \mathbb{R}$, which corresponds to $z \in \left[-1/\sqrt{1-U^2}, 1/\sqrt{1-U^2}\right]$. Also note that since $0 \leq \gamma \leq 1$, evidently $c_{g_1}, c_{g_2} \geq 0$, and $c_{g_3} \leq 0$, so the first two modes are right-going, and the third mode is left-going. When $\gamma = 0$, the x-component of the group velocity goes to zero for the last two modes, so we say these waves are *glancing*, or tangent to the boundary. The left eigenvectors of $M(z)$ are

$$Q(z) = \begin{pmatrix} Q^{\mathrm{I}} \\ Q^{\mathrm{II}} \end{pmatrix} = \begin{pmatrix} 2 & z(U+1) & z(U-1) \\ -2zU & 1+\gamma & 1-\gamma \\ -2zU & 1-\gamma & 1+\gamma \end{pmatrix}, \tag{4}$$

where Q^{I} is the first two rows and Q^{II} is the third row of Q. Thus the matrix Q decouples the equations into modes which have $c_g > 0$ and $c_g < 0$. Then the exact nonreflecting boundary conditions are

$$Q^{\mathrm{I}}\hat{q} = 0, \qquad \text{at } x = 0;$$
$$Q^{\mathrm{II}}\hat{q} = 0, \qquad \text{at } x = L.$$

These conditions are exact, but they are nonlocal, since γ is not a rational function of z.

The nonlocal boundary conditions may be shown to be well-posed. However, when we replace $\gamma(z)$ by a rational function approximation (such that we obtain a local boundary condition when we take the inverse Fourier-Laplace transform) an analysis of the well-posedness [8] shows that they boundary conditions are ill-posed for *any* rational function approximation for $\gamma(z)$. This is the situation reported by Giles [17] for the special case when $\gamma(z)$ is approximated by 1 (i.e. $\gamma(z)$ is approximated by the first term in its TSE).

However, it is possible maintain exact nonreflectivity *and* well-posedness by modifying the matrix Q^{I} as discussed in [18], and further amplified in [8]. We omit the details here, giving, for simplicity, only one particular choice for the modified matrix Q^{I}. The effect of making other choices will be discussed in [8].

Upon modification, the boundary conditions are,

$$\begin{aligned} E^{\mathrm{I}}\hat{q} &= 0, \qquad \text{at } x = 0; \\ E^{\mathrm{II}}\hat{q} &= 0, \qquad \text{at } x = L. \end{aligned} \tag{5}$$

where

$$\begin{aligned} E^{\mathrm{I}} &= \begin{pmatrix} 2 & z(U+1) & z(U-1) \\ z(1-U) & 1+\gamma & 0 \end{pmatrix} \\ E^{\mathrm{II}} &= \begin{pmatrix} -2zU & 1-\gamma & 1+\gamma \end{pmatrix} \end{aligned} \tag{6}$$

The right boundary condition is the same as before. Note that equation (5) was previously implemented for a particular approximation to $\gamma(z)$ in Goodrich and Hagstrom[18]. We have shown [8] that these boundary conditions are well-posed, *subject to certain constraints on the choice of the rational function used to approximate* $\gamma(z)$. These constraints are identical now to those determined by Trefethen and Halpern [16] for the simple wave equation. Conveniently, the constraints are met for many common categories of approximations. In particular, if the rational function approximation for $\gamma(z)$ is of degree (m, n) (i.e. the numerator and denominator are polynomials of degree m and n respectively), and is a Padé, Chebyshev, or least-squares approximation to the square root, the constraints are met if $m = n$ or $m = n + 2$.

We note in passing that in the case of supersonic flow ($U > 1$), all modes are either incoming our outgoing at a boundary. This implies that at the right boundary, there are no boundary conditions, while at the left boundary, all incoming waves may be specified. In the case of no incoming waves, then it suffices, in the continuous case, to set $q = 0$. This is not the case when we discretize the equations, as discussed in the next section, because the dispersive nature of the FD scheme gives waves which propagate in both direction, even in supersonic flow.

Finally, an analysis of the reflection coefficients [8] (e.g. the amplitude of an incoming wave as a function of an outgoing wave) shows that for any rational function approximation for $\gamma(z)$, the reflection coefficient for acoustic-acoustic reflections becomes one for the glancing waves where $\gamma = 0$. This is intuitively obvious as well, since it is impossible, locally,

to discern a left-going wave and right-going wave when $\gamma = 0$ since $\lambda_2 = \lambda_3$ at that point.

3 Discrete Boundary Conditions

The local boundary conditions for the continuous LEE must be discretized and combined with FD equations for the interior points. Typically, details of this implementation have not been discussed in the literature. Often implementation involves ad hoc boundary closures for FD schemes (one-sided schemes at the boundaries, and special schemes for near boundary nodes when large stencil interior schemes are used). Some specific schemes have been presented for compact FD schemes [20], and for DRP schemes [12]. However, a detailed analysis of accuracy and stability of these schemes has not been carried out when they are applied to various boundary conditions. In a more rigorous treatment, Carpenter et al. [21] have proposed particular boundary closures for high-order FD approximations to one-dimensional hyperbolic systems. These schemes are constructed to couple physical boundary conditions to the boundary closure of the FD scheme and can be proven to be stable. However, the boundary conditions they use do not account for the dispersive nature of the FD scheme and do not attempt to control the extent to which "spurious waves" are reflected by smooth waves.

Spurious waves (whose specific mathematical definition is discussed more fully below) are an artifact of the discretization, and have been extensively analyzed by Vichnevetsky [4]. In a previous paper [7], we showed how to develop closures for both downstream and upstream boundaries of one-dimensional linear hyperbolic equations. These maintain the desired order of accuracy of the interior scheme, are stable, and minimize reflection of smooth and spurious waves at artificial boundaries. The closure for a "downwind" boundary is similar to a closure of the FD scheme, at least up through the order of accuracy of the interior scheme. Upwind boundary closures, however, are not derivative operators but instead are designed to eliminate any reflection of upstream propagating spurious waves. The hierarchy of upwind conditions contains, as a special case, the upwind boundary conditions developed by Vichnevetsky [4].

We first briefly review this previous work and then show how it may be extended to the 2D local boundary conditions discussed in the previous section. Because the analysis is involved, we only outline the steps taken here. The details of the derivations are given in ref. [8]. We divide the analysis into three parts. In section 3.1, we consider a system of one-dimensional equations and apply the methods developed previously for the simple advection equation to obtain numerically nonreflecting boundary conditions. In section 3.2, we show how these results may be applied directly to supersonic flow. Finally, in section 3.3 we generalize these for application to the (subsonic) 2D equations of section 2.

3.1 One dimensional analysis

In the previous work, the simple scalar advection equation:

$$u_t = -u_x \tag{7}$$

in one dimension was analyzed. This equation admits solutions of the form

$$u(x,t) = \mathrm{e}^{\mathrm{i}(kx-\omega t)} \tag{8}$$

Inserting (8) into (7) gives the dispersion relation $\omega = k$, and therefore the phase velocity, $\mathrm{c}_p = \omega/k$, and the group velocity, $\mathrm{c}_g = d\omega/dk$, are both equal to 1.

The methodology used in this paper may be applied to any FD scheme, but we restrict our attention to the family of three-point central FD schemes given by

$$\alpha(u_x)_{j+1} + (u_x)_j + \alpha(u_x)_{j-1} = \frac{a}{h}(u_{j+1} - u_{j-1}). \tag{9}$$

where we have introduced a uniform grid in x, with mesh spacing h, and where $u_j(t)$ denotes the approximation to $u(jh,t)$. See [20] for a detailed discussion of compact difference schemes. For our purposes, it suffices to note that if $\alpha = 0$ and $a = 1/2$, we recover the standard second-order central difference scheme, and if $\alpha = 1/4$ and $a = 3/4$, we obtain the fourth-order Padé scheme. For the schemes given by (9), the modified dispersion relation is

$$\omega = \frac{2a \sin kh}{1 + 2\alpha \cos kh}.$$

which is plotted in Figure 1 for the second- and fourth-order schemes.

Note that well resolved waves ($kh \ll 1$) travel with the same group velocity as the continuous equation, but poorly resolved waves (increasing kh) travel with unphysical group velocities, and the most poorly resolved waves ($kh \approx \pi$) travel in the opposite direction ($\frac{d\omega}{dk} < 0$). These waves which travel in the wrong direction have been called *spurious numerical waves*, after Vichnevetsky [4].

Note also that for each frequency ω (below some critical value ω_c), there corresponds *two* values of

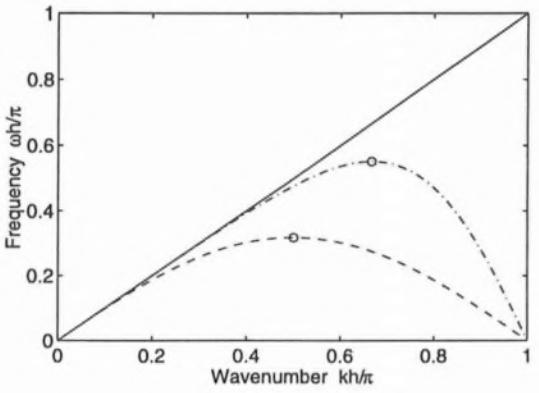

Figure 1: Dispersion relation for the simple advection equation, with exact derivative (———), second-order central difference scheme (----), and fourth-order Padé method (—·—).

k which satisfy the dispersion relation: a "physical" solution which travels in the correct direction ($c_g > 0$), and a "spurious" solution which travels in the opposite direction ($c_g < 0$), while for the continuous equation there was only one wavenumber k for each frequency ω. The two numerical solutions are uncoupled in the interior, but are (usually) coupled by the boundary conditions. Even in the simple one-way advection equation, physical waves reflect as spurious waves at the downwind boundary, with the opposite reflection at the upwind boundary.

If we wish to develop numerically "nonreflecting" boundary conditions, we must consider how the physical and spurious solutions are coupled at the boundary, and attempt to minimize this reflection. For later application to the 2D equations, it is useful to first generalize the previous analysis [7] to a *one-way system of equations*:

$$u_x = -Mu_t \tag{10}$$

in the domain $x \in (0, L)$, where u is a vector with n components, and M is an $n \times n$ positive-definite matrix. Note that if the matrix M were diagonalizable, we could decouple equation (10) into a system of n scalar equations using a similarity transform. This case is treated previously[7]. Here we need to consider the more general case where M is not necessarily diagonalizable. Inserting the FD approximation into equation (10), we obtain:

$$\alpha(-Mu_t)_{k+1} + (-Mu_t)_k + \alpha(-Mu_t)_{k-1} = \frac{a}{h}(u_{k+1} - u_{k-1}) \tag{11}$$

Now introduce a (normal mode) solution of the form

$$u_k(t) = \hat{u}\, e^{i\omega t}\kappa^k \tag{12}$$

where $\hat{u} \in \mathbb{R}^n$, $\omega \in \mathbb{R}$, and $\kappa \in \mathbb{C}$, so that

$$u_{k+1} = \kappa\, u_k$$

and (11) becomes

$$\left[\kappa^2(aI + \alpha i\omega hM) + \kappa(i\omega hM) - (aI - \alpha i\omega hM)\right]u = N(i\omega, \kappa)u = 0 \tag{13}$$

where $N(i\omega, \kappa)$ is the matrix in brackets. This linear system has nontrivial solutions only when

$$\det N(i\omega, \kappa) = 0 \tag{14}$$

Equation (14) is the dispersion relation for the discretized system. Let λ_j ($j = 1, \ldots, n$) be the eigenvalues of M (recall that all the eigenvalues presently have the same sign). Defining

$$\phi_j = \omega h \lambda_j, \qquad \text{for } j = 1, \ldots, n$$

and solving (14) for κ gives

$$\kappa^{\pm j} = \frac{-i\phi_j \pm \sqrt{4a^2 - \phi_j^2(1 - 4\alpha^2)}}{2(a + \alpha i\phi_j)} \tag{15}$$

where the $\kappa^{\pm j}$ satisfy

$$(\kappa^{\pm j})^2(a + \alpha i\phi_j) + \kappa^{\pm j} i\phi_j - (a - \alpha i\phi_j) = 0$$

for all $j = 1, \ldots, n$. Note that the number of roots (15) of the dispersion relation for the discretized equations is $2n$, while the dispersion relation of the non-discretized system has only n roots, corresponding to the n eigenvalues of M. Here, the κ^+ roots correspond to the "physical" solutions, and the κ^- roots correspond to the "spurious" modes mentioned in the previous section.

To distinguish the physical parts of the solution from the spurious parts, we consider a solution which is a superposition of modes of the form (12), and write the solution u_k at any grid point k as

$$u_k = \sum_{j=1}^{n} u_k^{+j} + \sum_{j=1}^{n} u_k^{-j}$$

where the $u_k^{\pm j}$ are normal modes of the form (12) which satisfy

$$N(i\omega, \kappa^{\pm j})u_k^{\pm j} = 0$$

for all $j = 1, \ldots, n$. Note that

$$u_{k+1}^{\pm j} = \kappa^{\pm j} u_k^{\pm j}$$

Because $M > 0$, all of the physical (u_k^{+j}) modes are rightgoing, and all of the spurious (u_k^{-j}) modes are leftgoing. Following our previous work [7] the exact *numerically nonreflecting* boundary condition at the left boundary ($k = 0$) is therefore

$$u_0^j = \frac{1}{\kappa^{-j}} u_1^j, \qquad \text{for all } j = 1, \ldots, n \tag{16}$$

which is equivalent to $u_0^{+j} = 0$. At the right boundary ($k = N$) the equivalent condition is

$$u_N^j = \kappa^{+j} u_{N-1}^j. \tag{17}$$

which gives $u_0^{-j} = 0$.

Because the $\kappa^{\pm j}$, given by equation (15), are not rational functions of the frequency ω, when the boundary conditions are transformed back into physical space they will be nonlocal in time. This is very similar to the situation which arose in deriving continuous boundary conditions for the 2D system in section 2. As mentioned earlier, we wish to derive approximate nonreflecting boundary conditions which are local in space and time. Extending our work in [7], we show in [8] that approximations to equations (16) and (17) can be obtained by setting:

$$c_1 h M \frac{\mathrm{d}u_0}{\mathrm{d}t} = \sum_{k=0}^{N_d} d_k u_k$$

for the point u_0, and

$$a_1 h M \frac{\mathrm{d}u_N}{\mathrm{d}t} = \sum_{k=0}^{N_b} b_k u_{N-k}$$

for the point u_N, where a_1, c_1 and the b_k and d_k are coefficients which are chosen to approximate the Taylor series expansion of Equations (16) and (17) about $\omega h = 0$. A large number of different schemes were tabulated in [7], and a subset of these are repeated in Table 1 for convenience. All the schemes presented in the table are computed for the fourth-order scheme.

It is helpful to introduce a more compact notation for the numerical boundary conditions. At the right (outflow) boundary, we write the boundary condition as

$$M \frac{\mathrm{d}u_N}{\mathrm{d}t} = \mathrm{d}_N^o u_N \tag{18}$$

Scheme:	bc0	bc1	bc2	bc4	bc6
Order:	–	2	3	5	7
a_1		1	2	12	72
b_0		−1	−3	−25	−175
b_1		1	4	48	424
b_2			−1	−36	−521
b_3				16	456
b_4				−3	−253
b_5					80
b_6					−11
c_1	1	−1	−2	−4	−8
d_0	0	3	9	45	189
d_1		3	12	120	792
d_2			3	132	1539
d_3				72	1704
d_4				15	1095
d_5					384
d_6					57

Table 1: Coefficients for numerically nonreflecting boundary conditions, with the interior scheme $a = 3/4$, $\alpha = 1/4$.

where d_N^o is the operator defined by

$$\mathrm{d}_N^o u_N = \frac{1}{a_1 h} \sum_{k=0}^{N_b} b_k u_{N-k}.$$

At the left (inflow) boundary, the numerical boundary condition is similarly written

$$M \frac{\mathrm{d}u_0}{\mathrm{d}t} = \mathrm{d}_0^i u_0 \tag{19}$$

where d_0^i is defined by

$$\mathrm{d}_0^i u_0 = \frac{1}{c_1 h} \sum_{k=0}^{N_d} d_k u_k.$$

Note that these boundary conditions apply only when M is positive-definite. Similar boundary conditions may also be derived for the case when M is negative-definite, and the coefficients merely change sign. When $M < 0$, the point u_N is an inflow boundary and the point u_0 is an inflow boundary, and the resulting boundary conditions are written

$$\begin{aligned} M \frac{\mathrm{d}u_N}{\mathrm{d}t} &= \mathrm{d}_N^i u_N \\ M \frac{\mathrm{d}u_0}{\mathrm{d}t} &= \mathrm{d}_0^o u_0 \end{aligned} \tag{20}$$

where d_N^i and d_0^o are defined by

$$\mathrm{d}_N^i u_N = -\frac{1}{c_1 h} \sum_{k=0}^{N_d} d_k u_{N-k}$$

$$\mathrm{d}_0^o u_0 = -\frac{1}{a_1 h} \sum_{k=0}^{N_b} b_k u_k.$$

3.2 2D Superonic Boundary Conditions

We noted at the end of section 2 that in the case of supersonic flow, the exact nonreflecting boundary conditions are simply that all the flow variables are zero at the right boundary, and no boundary conditions need be imposed at the downstream boundary. The analysis of the previous section shows that, in fact, spurious waves travel upstream even in supersonic flow, and so it is important to use a numerically nonreflecting boundary condition to avoid artificial communication upstream in the flow. For 2D supersonic flow, we merely apply the boundary conditions defined in equations (18) and (19) to the downstream and upstream boundaries, respectively. This can be first carried out in Fourier-Laplace space, by applying these to equation (2), and then taking the inverse Fourier-Laplace transform of the result. This procedure is entirely equivalent to interpreting the right hand sides of equations (18) and (19) as closures for the FD derivatives in the streamwise direction.

3.3 2D Subsonic Boundary Conditions

Now we show how the 2D boundary conditions of section 2 may be decoupled (approximately) into two systems of the form of equation (10), for which numerically nonreflecting boundary conditions are given by equation (20). Recall equation (2), which was the Fourier-Laplace transform (in y and $t' = t + y/V$) of the LEE, and that the well-posed local boundary conditions at $x = 0$ and $x = L$ for the continuous case were given by equation (5). Now define the square matrix

$$E = \begin{pmatrix} E^{\mathrm{I}} \\ E^{\mathrm{II}} \end{pmatrix}$$

and let $T(z)$ be the matrix of right eigenvectors of $M(z)$, such that

$$T^{-1}MT = \Lambda \equiv \begin{pmatrix} \Lambda^{\mathrm{I}} & 0 \\ 0 & \Lambda^{\mathrm{II}} \end{pmatrix}$$

where we have partitioned the eigenvalue matrix into blocks where $c_g > 0$ (Λ^{I}), and $c_g < 0$ (Λ^{II}). Now let

$$C \equiv ET = \begin{pmatrix} C^{\mathrm{I}} & D^{\mathrm{I}} \\ C^{\mathrm{II}} & C^{\mathrm{II}} \end{pmatrix}$$

where we have again partitioned the square matrix C into blocks. When the boundary condition is approximately nonreflecting, then the D^{I} and D^{II} blocks represent small error terms which identically vanish in the limit of the boundary conditions becoming exact. As an example, if the (m, n) Padé approximation is used for the square root, then the error is $O(z^{m+n+2})$ as $z \to 0$. In what follows, we neglect these small terms since it can be shown that none of the operations performed amplify the errors. Now let $g = E\hat{u}$. Then (2) becomes

$$\frac{\mathrm{d}}{\mathrm{d}x} E\hat{u} = -s(EME^{-1})E\hat{u} \tag{21}$$

$$\iff \frac{\mathrm{d}}{\mathrm{d}x} g = -s\Phi g \tag{22}$$

where

$$\Phi \equiv EME^{-1} = E(T\Lambda T^{-1})E^{-1} \tag{23}$$

$$= C\Lambda C^{-1} = \begin{pmatrix} \Phi^{\mathrm{I}} & 0 \\ 0 & \Phi^{\mathrm{II}} \end{pmatrix} \tag{24}$$

The eigenvalues of Φ^{I} and Φ^{II} are the same as the eigenvalues of Λ^{I} and Λ^{II}, respectively, so equation (22) is a system of two decoupled equations

$$\frac{\mathrm{d}}{\mathrm{d}x} g^{\mathrm{I}} = -s\Phi^{\mathrm{I}} g^{\mathrm{I}}$$

$$\frac{\mathrm{d}}{\mathrm{d}x} g^{\mathrm{II}} = -s\Phi^{\mathrm{II}} g^{\mathrm{II}}$$

where the first equation has purely right-going solutions ($\Phi^{\mathrm{I}} > 0$ for $z = 0$), and the second equation has purely left-going solutions ($\Phi^{\mathrm{II}} < 0$ for $z = 0$). Since the right-going and left-going modes are now decoupled, we may apply the numerical boundary conditions (18), (19), or (20) to each equation. Introducing a regular grid in x with mesh spacing h and letting g_k denote $g(x = kh)$, at the left boundary ($k = 0$) we obtain:

$$\begin{pmatrix} \mathrm{d}_0^i g_0^{\mathrm{I}} \\ \mathrm{d}_0^o g_0^{\mathrm{II}} \end{pmatrix} = s \begin{pmatrix} \Phi^{\mathrm{I}} g_0^{\mathrm{I}} \\ \Phi^{\mathrm{II}} g_0^{\mathrm{II}} \end{pmatrix} \tag{25}$$

and at the right boundary ($k = N$) we have

$$\begin{pmatrix} \mathrm{d}_N^o g_N^{\mathrm{I}} \\ \mathrm{d}_N^i g_N^{\mathrm{II}} \end{pmatrix} = s \begin{pmatrix} \Phi^{\mathrm{I}} g_N^{\mathrm{I}} \\ \Phi^{\mathrm{II}} g_N^{\mathrm{II}} \end{pmatrix} \tag{26}$$

Equations (25) and (26) can be further simplified to read:

$$D_L g_0 = \sum_{k=0}^{N_p} B_k^L g_k;$$

$$D_R g_N = \sum_{k=0}^{N_p} B_k^R g_{N-k}.$$

where

$$D_L = \begin{pmatrix} \mathrm{d}_0^i I & 0 \\ 0 & \mathrm{d}_0^o I \end{pmatrix} \qquad B_k^L = \begin{pmatrix} \frac{d_k}{c_1 h} I & \\ & \frac{-b_k}{a_1 h} I \end{pmatrix};$$

$$D_R = \begin{pmatrix} \mathrm{d}_N^o I & 0 \\ 0 & \mathrm{d}_N^i I \end{pmatrix} \qquad B_k^R = \begin{pmatrix} \frac{b_k}{a_1 h} I & \\ & \frac{-d_k}{c_1 h} I \end{pmatrix}.$$

where I denotes the identity matrix of appropriate dimension. Finally, these may be further transformed to

$$\begin{aligned} sEMq_0 &= \sum_{k=0}^{N_p} B_k^L E q_k \\ sEMq_N &= \sum_{k=0}^{N_p} B_k^R E q_{N-k}. \end{aligned} \tag{27}$$

These are numerically nonreflecting boundary conditions for the linearized Euler equations. They are approximate in two ways: first, the elements of the matrix E have rational function approximations to $\gamma(z)$, and second, the boundary closure operators of Equations (25) and (26) are approximate. However, both sets of approximations can be extended to arbitrary accuracy while maintaining stability.

Because the matrix E involves potentially high-order rational functions of $z \equiv ik/s$, the boundary conditions (27) are partial differential equations that involve potentially high-order mixed partials. In order to efficiently implement them, it is desirable to write the high order equations instead as systems of first order equations. Note that if the matrix E in (27) is a rational function of z, we may transform (27) into a system which is polynomial in z by multiplying each row by its least common denominator. For the boundary conditions (27), first we first clear denominators from both sides, obtaining (e.g. at left boundary)

$$sE'(z)M(z)\hat{q}_0 = \sum_{k=0}^{N_p} B_k^L E'(z)\hat{q}_k \tag{28}$$

where if the rational approximation to the square root is of degree (m, n), $E'(z)$ is a matrix polynomial of degree $p = \max\{m, n+1\}$ obtained by multiplying each row of $E(z)$ by its least common denominator. Then we define the matrix coefficients of powers of z:

$$\begin{aligned} E'(z)M(z) &= A_0 + zA_1 + \cdots + z^{p+1}A_{p+1} \\ E'(z) &= E_0 + zE_1 + \cdots + z^p E_p \end{aligned}$$

Finally, we define a sequence of state variables, c_1, c_2, $\cdots$, c_p, and implement (28), in real space (reverting from t' to t), as:

$$\begin{aligned} A_0\left(\frac{\partial q_0}{\partial t} + V\frac{\partial q_0}{\partial y}\right) &= \sum_{k=0}^{N_p} B_k^L E_0 q_k + \frac{\partial}{\partial y}(c_1 - A_1 q_0) \\ \frac{\partial c_j}{\partial t} + V\frac{\partial c_j}{\partial y} &= \sum_{k=0}^{N_p} B_k^L E_j q_k + \frac{\partial}{\partial y}(c_{j+1} - A_{j+1} q_0) \\ \frac{\partial c_p}{\partial t} + V\frac{\partial c_p}{\partial y} &= \sum_{k=0}^{N_p} B_k^L E_p q_k - \frac{\partial}{\partial y} A_{p+1} q_0 \end{aligned}$$

A similar equation (and set of state variables) can be defined for q_N. These are to be applied in combination with equation (1), with the difference formula (9) inserted (for points $1 < j < N-1$):

$$\begin{aligned} \alpha\frac{\partial q_{j+1}}{\partial t} + \frac{\partial q_j}{\partial t} + \alpha\frac{\partial q_{j-1}}{\partial t} \\ + \frac{a}{h}A(q_{j+1} - q_{j-1}) + B\frac{\partial q_j}{\partial y} = 0 \end{aligned}$$

If the approximation to $\gamma(z)$ is a rational function of degree (m, n), then the number of state variables required is $p = \max\{m, n+1\}$. Typically the number of grid points N in a computation would be much larger than p. Thus the additional computational cost for highly accurate boundary conditions is negligible.

4 Performance Tests

In this section we give the results of test problems which we have constructed to assess the accuracy of the various approximations which have been made in obtaining numerically nonreflecting boundary conditions. Specifically, we have used several different rational function approximations for $\gamma(z)$, and several of the different schemes for boundary closures reported in Table 1. In particular, we have considered the (2,0),(2,2),(4,4), and (8,8) Padé approximations to γ (Note that (2,0) Padé is the equivalent of the 2nd order TSE). Note also that the (4,4) scheme is equivalent to the (continuous version) of the boundary conditions in ref [18]. We also compare our schemes with Giles' boundary conditions. Finally, we have implemented a (4,4) rational function approximation which is chosen to interpolate the function $\gamma(z)$ at specific points (and will be referred to as "(4,4) Interp" in the discussions below). The interpolation points were chosen so that the performance of the approximation for nearly glancing waves would be improved. The specific points are $z = 0$, $\pm 1/4$, $\pm 1/2$, $\pm 3/4$, and ± 1.

In assessing the effects of using the numerical nonreflecting boundary closures, it is useful to compare our schemes with results which we obtain by using an "ad hoc" boundary closure. In this closure, we attempt to reproduce what we believe is the standard way of implementing nonreflecting boundary conditions. That is, we implement equation (5) directly and use a 4th-order explicit closure for the FD in the streamwise direction whenever necessary.

In all tests, we compute the solution on a 2D domain which is periodic in the y direction. The fourth order Padé scheme ($a = 3/4$, $\alpha = 1/4$) is used for the spatial derivatives, and 4th-order Runge-Kutta time advancement is used to advance all equations, boundary conditions, and state variables. We have observed that the CFL constraint of the scheme is unaffected by the boundary conditions or boundary closures, though we have no proof of this in the general case. The results given below all use a (maximum) CFL number of 1.

4.1 Convection of a vortex

In the first test, we consider the propagation of a vortex in a uniform stream with $U = 1/2$. To avoid the slowly decaying tangential velocity associated with finite circulation in 2D, we chose an initial "sombrero" vorticity distribution which has zero total circulation, given by:

$$\omega_z = \frac{1}{r}\frac{\partial}{\partial r}\left(r^2 e^{-(r/\alpha)^2}\right)$$

where $r = \sqrt{x^2 + y^2}$, in the computational domain $x \in [-5\alpha, 5\alpha]$, $y \in [-10\alpha, 10\alpha]$, with $Nx = 51$ and $Ny = 101$ points in the x- and y-directions, respectively. In the plots, lengths are given w.r.t. α, and time is normalized by α and the sound speed of the base flow.

Regardless of the choice of rational function, the continuous boundary conditions are exactly nonreflecting for the vorticity wave. Thus the vortex should merely propagate through the right boundary and subsequently the energy in the domain (or pressure or vorticity) should rapidly decay to zero. Thus this test is useful in assessing the choice of boundary closure from Table 1 and to compare these to results found by using the ad hoc 4th-order closure. Figure 2 shows the rms value of the vorticity (over x and y) as a function of time. Near $t = 10$, the vortex is passing through the right boundary. If there were no spurious reflections, then the energy within the domain would decrease to zero. However, the exiting vorticity produces a spurious vorticity wave which propagates upstream. The strength of this wave is evident between times 12 and 22, and is drastically reduced as the order of the boundary closure for the outgoing (smooth) waves (at $x = L$) is increased. The ad hoc boundary closure (which uses a fourth order one-sided FD scheme for closure), produces nearly the same results as boundary condition bc4 in this regime. However, the spurious wave eventually reflects at the upstream boundary, and the reflected energy is again greatly reduced by using the high order nonreflecting boundary closures. The ad hoc boundary closure clearly has a large reflection of this spurious wave at the inflow boundary.

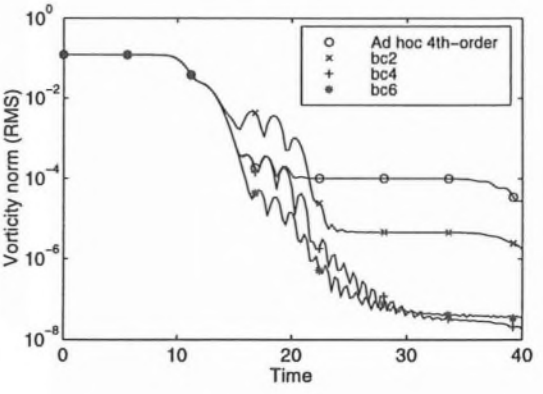

Figure 2: The rms vorticity in the computational domain as a function of time for several different nonreflecting boundary closures (see table 1).

4.2 Propagation of a pressure pulse

In the next test, an initially Gaussian distribution of pressure spreads out as a cylindrical acoustic wave in the domain with a uniform velocity $U = 1/2$. This problem (on both periodic [18] and nonperiodic domains [12]) has been suggested several times as a test of the efficacy of boundary conditions, since the numerical solution may be compared to the exact solution, which may be easily be reduced to a problem of quadrature. In the present case, we compare with the "exact" solution which we find by performing the computation on a much larger domain, until that time when it first becomes contaminated by reflections (physical or spurious) from the boundaries. This procedure is useful for isolating errors associated with the boundary conditions alone, since in the present case these can, for the most accurate boundary conditions, be smaller than other truncation errors.

The Gaussian pulse is initially given by $p = \exp -(r/\alpha)^2$, where α is the initial width of the pulse. Again the amplitude is unity, and α is used

for the length scale in the nondimensionalization. The grid is identical with the one for the vortex test discussed above. In Figure 3, pressure contours of the solution are plotted at several different times and show the propagation of the wave. Since the domain is periodic, waves from images of the initial condition are evident beginning at time $t = 10$. After an earlier time of $t = 6$, we see that a significant component of the wave motion corresponds to nearly glancing waves. As discussed at the end of section 2, all of the rational function approximations in the continuous boundary conditions give pure reflection in the limit of glancing waves. (Note that for $U = 1/2$, glancing waves have wavefronts at an angle $\sin^{-1} U = 30°$ to the horizontal.)

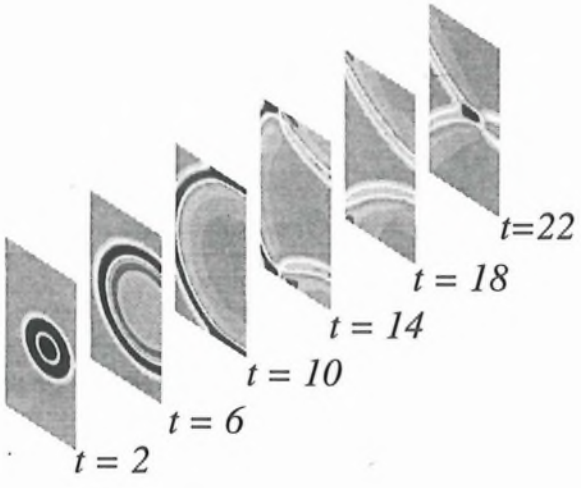

Figure 3: Initial pressure pulse. Contours of the pressure (min -0.1, max 0.1, incr 0.01) at several instants in time for Pade (2,2) approximation with d^i from scheme bc4 and d^o from scheme bc4

In Figure 4, we show the rms value (over the domain) of the error between the exact and numerical solution as a function of time for several different rational function approximations for $\gamma(z)$. All of these are implemented using the nonreflecting boundary closure bc4 for the incoming waves and outgoing waves at each boundary. Note the log scale in the plot. At early times $t < 5$ when the acoustic wave is leaving the right boundary at nearly normal incidence, the error in all the boundary conditions is very small, but increasing as the wave near the right boundary rotates towards glancing incidence near $t = 6$. For the most accurate schemes, the error for times less than $t = 5$ is apparently dominated

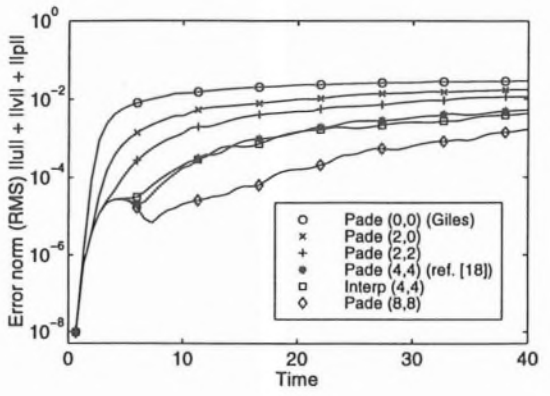

Figure 4: For a smooth pressure pulse, the rms error in the pressure is plotted as a function of time for several different rational function approximations for $\gamma(z)$ all with d^i from scheme bc4 and d^o from scheme bc4.

by reflection of spurious waves (this is demonstrated more clearly in figure 5 below). For early times, the (8,8) Padé approximation has error roughly 3 orders of magnitude below the (0,0) Padé approximation which is equivalent to Giles [17] as noted above. The interpolated (4,4) boundary condition is roughly equivalent to the (4,4) Padé condition, but better for long times since it better resolves nearly tangential waves.

In Figure 5, we again plot the error between the exact and numerical solution, but for different numerical boundary closures, all using the (2,2) Padé approximation for $\gamma(z)$. At early times, the benefit

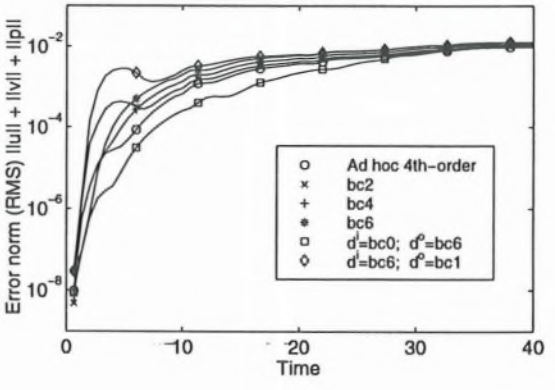

Figure 5: For a smooth pressure pulse, the rms error in the pressure is plotted as a function of time for several boundary closures all with the (2,2) Padé approximation for $\gamma(z)$.

of using the higher-order closures for the outgoing

waves is evident. The initial "bump" in the curves centered around $t = 4$ is the spurious wave reflecting from the right boundary as noted above. The amplitude of this error is is decreased as the order of accuracy of the scheme used for the outgoing waves (the d^o operator in equation (26)) is increased. That is, using scheme bc6 for d^o gives the best results, and using the scheme bc1 for d^o gives the worst results.

For $t > 5$, the error is dominated by waves near glancing (for which the continuous boundary condition performs most poorly), and we see that the results become much less sensitive to the choice of closure for the outgoing waves. Instead, the error becomes sensitive to the choice of closure for the incoming waves. In fact, for the glancing waves, it is evident that the highest-order schemes for the incoming waves (d^i) *perform the worst.*

This can be understood by looking at the structure of the coefficients in table 1. Note that application of the operator d^i to a sawtooth wave (i.e. a wave which alternates between plus and minus 1 every other grid point) yields 0, while the application of the operator d^o to a constant (smooth wave), yields 0. When applied to the wrong wave (i.e apply d^i to the smooth wave and d^o to the sawtooth wave), both operators give a very large number, and this number is increased as the order of scheme is increased, since the magnitude of the coefficients increases as we move to the right in table 1

Now, at glancing incidence, the ability to distinguish between incoming and outgoing modes is degraded as the approximation to $\gamma(z)$ becomes worse, and therefore both operators d^i and d^o are (wrongly) applied to both incoming and outgoing disturbances which are near glancing incidence. We are applying the wrong operator to each wave. Since the most nearly glancing waves are *smooth* waves that have not yet reflected off the boundary, the main error comes from applying d^i to the smooth wave. Thus the error increases as the order of accuracy of the operator d^i is increased.

This behavior is further confirmed by noting that in the figure we have included the results for the 4th-order "ad hoc" boundary closure. We have also shown results for an incoming scheme which we label as scheme bc0. This scheme is one for which the coefficients d_k are all set identically to zero. Note that this is not equivalent to the "ad hoc" boundary closure. The application of the bc0 scheme for d^i is seen to give the best results for long time when most of the waves are near glancing incidence.

To further illustrate this point, it is interesting to simulate the effect of having a poorly resolved initial condition to see if the high-order incoming wave boundary closures are effective for this case. To do this, we initialize the calculation with the pressure pulse but we multiply it by a sawtooth wave which oscillates between plus and minus 1 every other grid point. Thus we shift the energy from the well-resolved waves near $kh = 0$ in Figure 1 to the poorly resolved waves at $kh = \pi$. The "exact" solution is again obtained by solving the same problem on the larger domain. The solution (not shown) is nonphysical, but is, in essence, similar to that of the well-resolved pulse, except that the x-component of the group velocity is negative and about 3 times (i.e. the slope of the dispersion relation of figure 1 near $kh = \pi$) the speed of the smooth acoustic waves of figure 3.

The error for this case is plotted in figure 6 for the same schemes considered in figure 5. The curves show exactly the opposite trends as the previous case, with the "ad hoc" and bc0 closures performing most poorly. For long time, when the sawtooth wave is again near glancing incidence to the boundaries, we see the largest error is generated by using the schemes with the highest-order operator for the smooth waves.

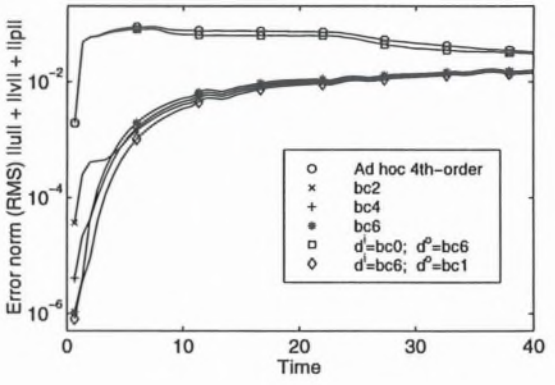

Figure 6: For a sawtooth pressure pulse, the rms error in the pressure is plotted as a function of time for several boundary closures all with the (2,2) Padé approximation for $\gamma(z)$.

Both of the last tests really demonstrate the extreme possibilities for the performance of the boundary conditions. In both cases, the highest-order nonreflecting boundary closures (e.g. scheme bc6) give the best results for early times before the approximation to $\gamma(z)$ breaks down (when most of the waves in the domain are at nearly glancing incidence to the boundaries). Many physically realistic acoustic fields will not involve waves near glancing incidence and in those cases one would expect uniformly bet-

ter results as the accuracy of the approximation is increased, and as the order-of-accuracy of the non-reflecting boundary closures is increased.

5 Summary

We have developed a framework for constructing local, strongly well-posed boundary conditions for FD solutions of the linearized Euler equations. These boundary conditions take explicit account of the dispersive character of the FD approximation, and are designed to minimize the reflection of spurious waves at the boundaries. As such, they are dependent on the particular FD scheme, and we have used a 3 point Padé centered FD scheme to illustrate the analysis. The analysis leads to different boundary closures which need to be applied to incoming and outgoing waves at each boundary.

The boundary conditions rely on a rational function approximation to the function $\gamma(z)$ which is obtained when waves are decomposed into modes with positive and negative group velocites in Fourier space. As in previous boundary conditions for the simple wave equation [16], we have shown that a variety of rational function approximations lead to stable, well-posed boundary conditions. The scheme can thus be extended to arbitrarily high order-of-accuracy.

In general, various tests of the boundary conditions show that the highest-order schemes (and most accurate rational function approximations) perform the best. However, there can exist situations where the higher-order boundary closures give inferior results to low-order boundary closures and certain other ad hoc boundary closures. These situations always involve waves which are near glancing incidence to the boundary where the error in the rational function approximation to $\gamma(z)$ is a maximum. If such waves are expected in practical calculations, then one should use the lower-order closures for the incoming waves.

In the future, we intend to apply these boundary conditions to more complicated problems. In particular, there is an urgent need for accurate boundary conditions when the equations near the boundary are either nonlinear (as in a turbulent outflow) or have non-constant coefficients. We hope that providing a general framework, wherein *all the errors due to artificial boundary conditions* have been analyzed, will aid in the development of techniques for more complex flows.

Acknowledgements

This research was supported in part by the National Science Foundation under grant CTS-9501349 with technical monitor Dr. Roger Arndt, and we also acknowledge the recent support of AFOSR under grant F49620-98-1-0095 with technical monitor Dr. Mark Glauser.

References

[1] Sanjiva K. Lele. Computational aeroacoustics: A review. AIAA Paper 97-0018, January 1997.

[2] Christopher K. W. Tam. Computational aeroacoustics: Issues and methods. *AIAA Journal*, 33(10):1788–1796, October 1995.

[3] T. Colonius, S. K. Lele, and P. Moin. Boundary conditions for direct computation of aerodynamic sound generation. *AIAA Journal*, 31(9):1574–1582, September 1993.

[4] Robert Vichnevetsky. Wave propagation analysis of difference schemes for hyperbolic equations: A review. *International Journal for Numerical Methods in Fluids*, 7:409–452, 1987.

[5] Lloyd N. Trefethen. Group velocity interpretation of the stability theory of Gustafsson, Kreiss, and Sundstrom. *Journal of Computational Physics*, 49:199–217, 1983.

[6] Christopher K. W. Tam and Jay C. Webb. Radiation boundary condition and anisotropy correction for finite difference solutions of the helmholtz equation. *Journal of Computational Physics*, 113(1):122–133, 1994.

[7] Tim Colonius. Numerically nonreflecting boundary and interface conditions for compressible flow and aeroacoustic computations. *AIAA Journal*, 35(7):1126–1133, 1997.

[8] C. W. Rowley and Tim Colonius. Discrete nonreflecting boundary conditions for linear hyperbolic systems. Manuscript in preparation. Preliminary version available at http://green.caltech.edu/tc.html. Department of Mechanical Engineering, California Institute of Technology, May 1998.

[9] Dan Givoli. Non-reflecting boundary conditions. *Journal of Computational Physics*, 94:1–29, 1991.

[10] Christopher K. W. Tam. Advances in numerical boundary conditions for computational aeroacoustics. AIAA Paper 97-1774, 1997.

[11] Marcus J. Grote and Joseph B. Keller. Exact nonreflecting boundary conditions for the time dependent wave equation. *SIAM Journal of Applied Mathematics*, 55(2):207–307, April 1995.

[12] Christopher K. W. Tam and Jay C. Webb. Dispersion-relation-preserving finite difference schemes for computational acoustics. *Journal of Computational Physics*, 107:262–281, 1993.

[13] R. Hixon, S.-H Shih, and Reda R. Mankbadi. Evaluation of boundary conditions for computational aeroacoustics. *AIAA Journal*, 33(11):2006–2012, November 1995.

[14] Bjorn Engquist and Andrew Majda. Absorbing boundary conditions for the numerical simulation of waves. *Mathematics of Computation*, 31(139):629–651, 1977.

[15] Bjorn Engquist and Andrew Majda. Radiation boundary conditions for acoustic and elastic wave calculations. *Communications on Pure and Applied Mathematics*, 32:313–357, 1979.

[16] Lloyd N. Trefethen and Laurence Halpern. Well-posedness of one-way wave equations and absorbing boundary conditions. *Mathematics of Computation*, 47(176):421–435, October 1986.

[17] Michael B. Giles. Non-reflecting boundary conditions for euler equation calculations. *AIAA Journal*, 28(12):2050–2058, 1990.

[18] John W. Goodrich and Thomas Hagstrom. A comparison of two accurate boundary treatments for computational aeroacoustics. AIAA Paper 97-1585, 1997.

[19] Thomas Hagstrom. *On High-Order Radiation Boundary Conditions*, pages 1–21. 1996.

[20] Sanjiva K. Lele. Compact finite difference schemes with spectral-like resolution. *Journal of Computational Physics*, 103(1):16–42, November 1992.

[21] Mark H. Carpenter, David Gottlieb, and Saul Abarbanel. Time-stable boundary conditions for finite-difference schemes solving hyperbolic systems: Methodology and applicatio n to high-order compact schemes. *Journal of Computational Physics*, 111:220–236, 1994.